INT. J. REMOTE SENSING, 2001, VOL. 22, NO. 2 & 3, 249–273

Remote sensing of phytoplankton pigments: a comparison of empirical and theoretical approaches

S. SATHYENDRANATH†‡, G. COTA§, V. STUART†, H. MAASS† and T. PLATT‡

†Department of Oceanography, Dalhousie University, Halifax, Nova Scotia, Canada B3H 4J1
‡Biological Oceanography Division, Bedford Institute of Oceanography, Box 1006, Dartmouth, Nova Scotia, Canada B2Y 4A2
§Center for Coastal Physical Oceanography, Old Dominion University, Norfolk, Virginia 23529, USA

(*Received 2 February 1998; in final form 10 June 1999*)

Abstract. Algorithms that have been used on a routine basis for remote sensing of the phytoplankton pigment, chlorophyll-*a*, from ocean colour data from satellite sensors such as the CZCS (Coastal Zone Color Scanner), SeaWiFS (Sea Viewing Wide Field-of-View Sensor) and OCTS (Ocean Colour and Temperature Scanner) are all of an empirical nature. However, there exist theoretical models that allow ocean colour to be expressed as a function of the inherent optical properties of seawater, such as the absorption coefficient and the backscattering coefficient. These properties can in turn be expressed as functions of chlorophyll-*a*, at least for the so-called Case 1 waters in which phytoplankton may be considered to be the single, independent variable responsible for most of the variations in the marine optical properties. Here, we use such a theoretical approach to model variations in ocean colour as a function of chlorophyll-*a* concentration, and compare the results with some empirical models in routine use. The parameters of phytoplankton absorption necessary for the implementation of the ocean colour model are derived from our database of over 700 observations of phytoplankton absorption spectra and concurrent measurements of phytoplankton pigments by HPLC (High Performance Liquid Chromatography) techniques. Since there are reports in the literature that significant differences exist in the performance of the algorithms in polar regions compared with lower latitudes, the model is first implemented using observations made at latitudes less than 50°. It is then applied to the Labrador Sea, a high-latitude environment. Our results show that there are indeed differences in the performance of the algorithm at high latitudes, and that these differences may be attributed to changes in the optical characteristics of phytoplankton that accompany changes in the taxonomic composition of their assemblages. The sensitivities of the model to assumptions made regarding absorption by coloured dissolved organic matter (or yellow substances) and backscattering by particles are examined. The importance of Raman scattering on ocean colour and its influence on the algorithms are also investigated.

1. Introduction

The first sensor to monitor ocean colour from space, the Coastal Zone Color Scanner (CZCS), was launched by NASA (National Aeronautics and Space Administration) in 1978. It functioned as a proof-of-concept satellite until 1986. The

International Journal of Remote Sensing
ISSN 0143-1161 print/ISSN 1366-5901 online
http://www.tandf.co.uk/journals

demise of the CZCS left a void in the stream of ocean colour data from space. This void was not filled until almost a decade later, when three satellites were launched in quick succession carrying the following sensors: the Modular Optoelectronic Scanner (MOS), sponsored jointly by Germany and India, launched in March 1996; the Japanese Ocean Colour and Temperature Scanner (OCTS) and the French sensor called Polarisation and Directionality of the Earth's Reflectances (POLDER), both launched in August 1996 and operated until June 1997; and the Sea Viewing Wide Field-of-View Sensor (SeaWiFS), a NASA mission launched in August 1997. Several other ocean colour sensors are planned for launch in the next few years. These new sensors have benefited from the CZCS experience, and have incorporated several spectral and radiometric improvements over the CZCS. If we are to exploit the full potential of these advanced sensors, we also need to develop new algorithms that make use of the enhanced capabilities of the sensors. It would also be desirable to provide a sound theoretical basis for these algorithms, so that we can improve our understanding of their strengths and weaknesses.

The standard data processing strategy of these sensors (with the notable exception of MOS) is to correct the data for atmospheric noise in order to obtain water-leaving radiance. The water-leaving radiance is then processed to obtain a measure of pigment concentration in the surface waters. The in-water algorithms used for this purpose are often empirical in nature. Conversely, theoretical models of ocean colour exist that express water-leaving radiance as a function of two inherent optical properties of the water column: the absorption coefficient and the backscattering coefficient. However, an early attempt to implement an algorithm based on theoretical considerations showed some systematic differences between the model results and the empirical relationships in common use for processing CZCS data (Sathyendranath and Platt 1989), which has somewhat limited the algorithm's applicability.

In this paper we present a refined version of this model for ocean colour. The major modifications of the model are that it incorporates Raman scattering by pure water and the representations of absorption by pure water and by phytoplankton have been improved. Furthermore, the implementation of phytoplankton absorption is based on an analysis of a large body of data collected by our group. The model outputs are then compared against empirical relationships in common use for processing data from CZCS (Gordon *et al.* 1983), OCTS (Kishino *et al.* 1995, NASDA 1997) and SeaWiFS (O'Reilly *et al.* 1998). We also try to understand the causes of discrepancies between model and empirical relationships, when they exist, by studying the sensitivity of the model to the various assumptions and simplifications used in its implementation.

There have been reports (Mitchell and Holm-Hansen 1991, Mitchell 1992, Sullivan *et al.* 1993) of significant differences between the performance of the CZCS algorithm in high latitudes and in lower latitudes. Therefore, our model is implemented here first with parameters of phytoplankton absorption that are established for low and mid latitudes (latitude less than 50°). We then test the performance of the resulting model against data collected in a high-latitude environment (the Labrador Sea) and examine whether the differences observed can be explained on the basis of the absorption properties of the different phytoplankton assemblages encountered in these waters.

2. Ocean colour model and its implementation

Intrinsic ocean colour is determined by spectral variations in reflectance at the sea surface. Reflectance is defined as the ratio of upwelling irradiance to downwelling

irradiance at the same depth, so that we have:

$$R(\lambda, z) = \frac{E_u(\lambda, z)}{E_d(\lambda, z)} \tag{1}$$

where $R(\lambda, z)$ is the reflectance at wavelength λ and depth z, $E_u(\lambda, z)$ is the upwelling irradiance at the same wavelength and depth, and $E_d(\lambda, z)$ is the corresponding downwelling irradiance.

As implemented here, the model is designed for retrieval of phytoplankton pigment concentrations using remotely sensed data in the blue–green part of the spectrum. In constructing the model, it is assumed that reflectance at the sea surface can be generated by Raman scattering and by elastic scattering. These two components of ocean colour were treated as follows.

The elastic scattering component of reflectance (R^E) at the sea surface was computed as in the work of Sathyendranath and Platt (1997), which is also consistent with a number of earlier models (Gordon *et al.* 1975, Morel and Prieur 1977, Ăas 1987):

$$R^E(\lambda, 0) = r\left(\frac{b_b(\lambda)}{[a(\lambda) + b_b(\lambda)]}\right) \tag{2}$$

where r is a proportionality factor and $b_b(\lambda)$ and $a(\lambda)$ are the backscattering and absorption coefficients at wavelength λ. There is recent evidence that the proportionality factor r may vary with the zenith angular distribution of the light field underwater, as well as with the shape of the phase function for scattering (Gordon 1989, Kirk 1989, Morel and Gentili 1993, Sathyendranath and Platt 1997). There is also some evidence that it may vary with wavelength (Morel and Gentili 1991), but in the implementation presented here we have taken r to be wavelength independent.

Reflectance due to Raman scattering was computed using the model of Sathyendranath and Platt (1998), which has a first-order term accounting for a single Raman upward scatter (R^R) and two second-order terms accounting for a combination of elastic and Raman scattering events (R^{RE} and R^{ER}). The total reflectance at the sea surface was then computed as the sum of the contributions due to elastic and Raman scattering. The magnitude of the Raman scattering coefficient and the wavelength dependence of Raman scattering were modelled following the experimental results of Bartlett *et al.* (1998).

The attenuation coefficients for downwelling irradiances, $K_d(\lambda)$, and for upward transmission of scattered irradiance, $\kappa(\lambda)$, required in the calculation of the Raman component were modelled as simple functions of a and b_b:

$$K(\lambda) = \frac{a(\lambda) + b_b(\lambda)}{\mu_d} \tag{3}$$

and

$$\kappa(\lambda) = \frac{a(\lambda) + b_b(\lambda)}{\mu_u} \tag{4}$$

where μ_d and μ_u are the mean cosines for downwelling and upwelling lights respectively. In computing μ_d and μ_u we assumed that the source of all downwelling irradiance was the Sun at 30° zenith angle above water, and that the upwelling irradiance was uniformly diffuse (that is, $\mu_d = 0.93$ and $\mu_u = 0.5$). Note that the

attenuation coefficient κ differs from the diffuse attenuation coefficient for upwelling irradiance K_u discussed later on in this paper. The parameter K_u determines the rate of decrease of upwelling irradiance with *increasing* depth, whereas κ determines the rate of decrease of upwelling irradiance with *decreasing* depth (Kirk 1989). According to the model of Sathyendranath and Platt (1997, 1998) the proportionality factor r in equation (2) is a function of the shape factor for scattering. This parameter was set to unity in the calculations presented here.

The backscattering and absorption coefficients were expressed as the sum of their components:

$$b_b(\lambda) = b_{bw}(\lambda) + b_{bp}(\lambda) \tag{5}$$

and

$$a(\lambda) = a_w(\lambda) + a_y(\lambda) + a_p(\lambda) \tag{6}$$

where the subscript w stands for pure seawater, p for particulate material and y for yellow substances or gelbstoff. Computations of backscattering and absorption coefficients are now discussed in turn.

2.1. *Backscattering coefficient*

Scattering by water was computed according to Morel (1974), and since scattering by water molecules is symmetric, backscattering is 50% of the total scattering by water.

Scattering by particles was modelled as follows. First, particle scattering was computed at 660 nm using an equation from Loisel and Morel (1998):

$$b_p(660) = 0.407 C^{0.795} \tag{7}$$

where C is the concentration of the main phytoplankton pigment, chlorophyll-*a*. This is a modification of a similar equation presented by Gordon and Morel (1983). The next step is to specify the wavelength dependence of particle scattering. According to Morel (1973), for a Junge-type particle size distribution in the ocean with an exponent of $-m$, the wavelength dependence of scattering follows a $\lambda^{(3-m)}$ law. Several workers (Bader 1970, Brun-Cottan 1971, Sheldon *et al.* 1972, Jonasz 1983, Platt *et al.* 1984) have reported Junge-type particle size distributions in oceanic waters, with the exponent m varying between 3 and 5. This would imply that the wavelength dependence of scattering would obey a λ^n law, with $n = 3 - m$ varying between 0 and -2. Sathyendranath *et al.* (1989) reported, when comparing their model with their observations, that the values of n which gave the best fit with observations varied between 0 and -2, with the higher values appearing predominantly in oligotrophic waters. Ulloa *et al.* (1994) argued that there is evidence in the literature that the value of m increases (the slope becomes more negative) for increasingly oligotrophic waters, consistent with the results of Sathyendranath *et al.* (1989). Note that this change in slope implies that the abundance of small particles (consisting of bacteria, viruses and other organic particles) relative to phytoplankton concentration would be greater in oligotrophic waters than in eutrophic waters. In the model calculations presented here, the spectral variations in particle scattering were estimated by setting

$$b_p(\lambda) = b_p(660)(660/\lambda)^{-n} \tag{8}$$

and the value of n was allowed to decrease with chlorophyll-*a* concentration, by setting

$$n = \log_{10} C \tag{9}$$

where C is measured in mg Chl-*a* m^{-3}, and the wavelength λ in nm. Ciotti *et al.* (1999) also allowed n to vary as some function of $\log C$.

The final step in modelling particle backscattering is to compute the backscattering ratio for particles $\tilde{b}_{bp}$, which is defined as the ratio of backscattering by particles to the total scattering coefficient by particles, such that we have $b_{bp}(\lambda) = \tilde{b}_{bp} b_p(\lambda)$. We used the equation of Ulloa *et al.* (1994) to estimate $\tilde{b}_{bp}$:

$$\tilde{b}_{bp} = 0.01\,(0.78 - 0.42 \log_{10} C) \tag{10}$$

This equation was obtained by fitting a curve to the results of Sathyendranath *et al.* (1989) on the variability in $\tilde{b}_{bp}$ as a function of chlorophyll-*a*. Furthermore, this equation is consistent with the theoretical calculations of Ulloa *et al.* (1994), which showed that the backscattering ratio of particles would be greater for higher values of m, the exponent of the Junge-type particle distribution. It follows that $\tilde{b}_{bp}$ would be greater in oligotrophic waters than in phytoplankton-rich waters, if indeed m increases with oligotrophy. Note that equation (10) also implies that $\tilde{b}_{bp}$ is wavelength independent, which is also in accordance with the theoretical results of Ulloa *et al.* (1994). We set upper and lower limits on $\tilde{b}_{bp}$, to avoid too-high or too-low values: explicitly, $0.0005 \leqslant \tilde{b}_{bp} \leqslant 0.01$. Thus, the backscattering coefficient at wavelength λ was computed as:

$$b_b(\lambda) = 0.5 b_w(\lambda) + \tilde{b}_{bp} b_p(\lambda) \tag{11}$$

2.2. *Total absorption coefficient*

Absorption by pure (sea) water was estimated according to Pope and Fry (1997). Since the model presented here is meant for use in Case 1 waters (those waters in which phytoplankton and covarying substances may be assumed to be the principal agents responsible for variations in the optical properties of the water, as defined by Morel (1980)), we have taken absorption by yellow substances to covary with phytoplankton absorption, similarly to the approach used in the absorption model of Prieur and Sathyendranath (1981), and set $a_y(440) = 0.3 a_p(440)$. The spectral variation of absorption by yellow substances was described using an exponential function with an exponent of -0.014, based on the results of Bricaud *et al.* (1981).

The development of the model component that evaluates absorption by phytoplankton was based on a compilation of phytoplankton absorption spectra measured by our group using the filter technique (Stuart *et al.* 1998, Sathyendranath *et al.* 1999), and corresponding measurements of pigment concentrations using the HPLC (High Performance Liquid Chromatography) technique as described in Head and Horne (1993). The data used in this analysis were collected during 13 cruises (table 1, figure 1). Since there is some evidence that the performance of some algorithms for chlorophyll retrieval from ocean colour data is significantly different in high latitudes compared with that in low latitudes (Mitchell and Holm-Hansen 1991, Mitchell 1992, Sullivan *et al.* 1993, Fenton *et al.* 1994), we used data collected only at latitudes less than 50°. Some 716 samples were used. For each of the wavelengths used in standard CZCS, OCTS and SeaWiFS algorithms, and for the corresponding Raman

Table 1. Summary of datasets available for the analysis presented in this paper, including dates, locations and numbers of observations. Only samples which had both absorption and HPLC chlorophyll-*a* data from latitudes south of 50°N are represented in this table. Total number of observations is 716.

Expedition	Year	Period	Region	*n*
JGOFS 96	1996	15 May–30 May	NW Atlantic	10
JGOFS 97	1997	12 May–13 May	NW Atlantic	4
Hudson Jun. 98	1998	24 Jun–08 Jul	NW Atlantic	6
Sonne 97	1997	15 Jun–07 Jul	Arabian Sea	91
Meteor 96	1996	10 Sep–03 Oct	NE Atlantic	33
Hudson Apr. 97	1997	18 Apr–28 Apr	Scotian Shelf	20
Hudson Oct. 97	1997	26 Oct–08 Nov	Scotian Shelf	24
Arabesque 1	1994	28 Aug–30 Sep	Arabian Sea	109
Arabesque 2	1994	17 Nov–15 Dec	Arabian Sea	95
Georges Bank 89	1989	11 Sep–21 Sep	Georges Bank	120
Sonne 95	1995	11 May–26 June	SE Pacific	140
Vancouver	1996	05 Mar–14 Mar	Off Vancouver Island	36
WOCE 93	1993	07 Apr–10 May	Trans Atlantic	28

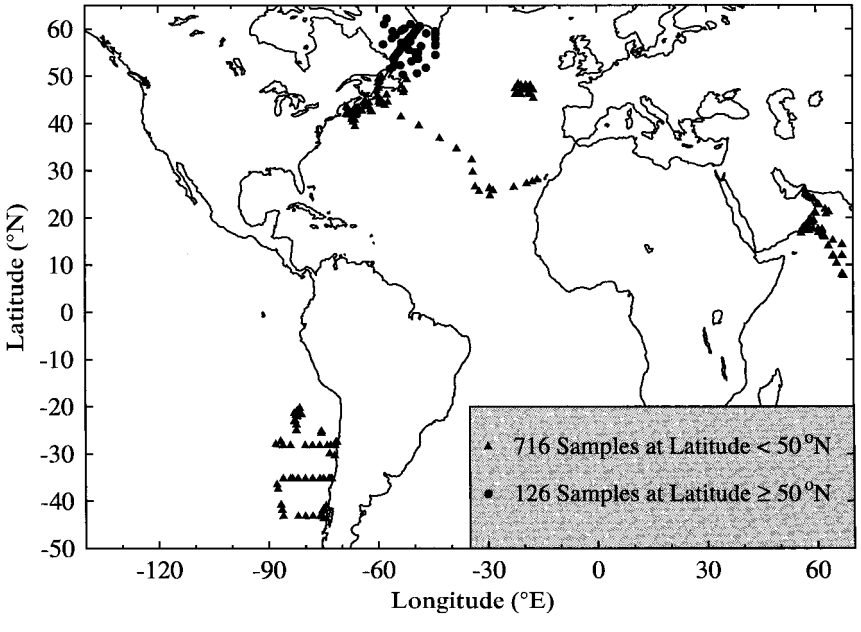

Figure 1. Map showing the location of the stations where the phytoplankton absorption data and the corresponding pigment measurements were made. Note that only data from latitudes south of 50°N were used in the development of the low and mid latitude model. Further details regarding the cruises in which the data were collected are given in table 1.

wavelengths, the absorption coefficient of phytoplankton pigment was plotted against chlorophyll-*a* concentration. A Michaelis–Menten equation of the form:

$$a_p(\lambda) = \frac{a_m a_m^* C}{a_m + a_m^* C} \tag{12}$$

was fitted to the data, where the parameter a_m defines the asymptotic maximum value of the absorption coefficient and a_m^* defines the maximum slope of the curve near the origin (maximum specific absorption coefficient). As an example, figure 2 shows a plot of the phytoplankton absorption coefficient at 443 nm as a function of C, and the equation fitted to the data. Table 2 gives the parameters of the fit for all the wavelengths used in the calculations presented here.

3. Comparison of empirical algorithms and model implementation for low and mid latitudes

The model described above was used to generate theoretical values of reflectances at the sea surface, for pigment concentrations ranging from 0.01–40 mg Chl-a m^{-3}. The results were then used to calculate reflectance ratios of the type used in empirical algorithms for processing CZCS, OCTS and SeaWiFS data. The results are plotted in figure 3, together with the empirical relationships.

We recognize that the water-leaving radiances derived from satellite data are not identical to the reflectances computed here. The differences arise from two sources. (i) The satellite data pertain to fluxes above the water, whereas the reflectance values computed here are for fluxes just below the sea surface. (ii) Satellite data yield normalized radiances (fluxes per unit area per unit steradian), whereas the reflectance model presented here deals with irradiance (fluxes per unit area). Therefore, when reflectance ratios are treated as analogous to radiance ratios in ocean colour models, there is an implicit assumption that the factors linking upwelling radiance above water to upwelling irradiance below water are spectrally neutral, and therefore cancel out when ratios are taken (Sathyendranath and Morel 1983).

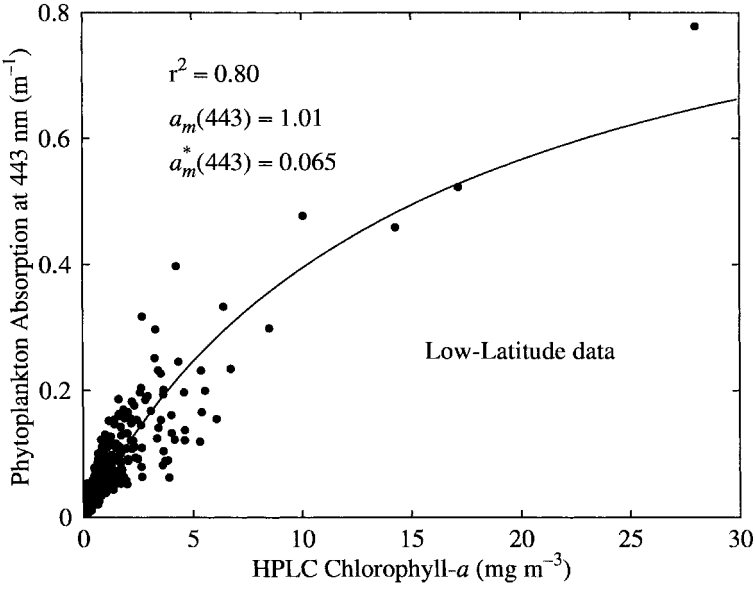

Figure 2. An example of the absorption and pigment data and the fit of the Michaelis–Menten equation (equation (12)) to the data. The values of the fitted parameters and the coefficient of determination (r^2) are also given. Similar fits were made for each of the wavelengths used in the algorithms (see table 2 for the fitted parameter values for each wavelength).

Table 2. The parameters a_m (m^{-1}) and a_m^* ($m^2\,mg(Chl\text{-}a)^{-1}$) of equation (12) for three datasets as a function of wavelength. Parameter values are given for each of the wavelengths used in the algorithms presented here (lower member of each pair), and for their corresponding Raman wavelengths (upper member).

	Low latitude data		Diatom bloom		Prymnesiophyte bloom	
λ (nm)	a_m	a_m^*	a_m	a_m^*	a_m	a_m^*
386	1.252	0.0509	0.4956	0.0269	0.2517	0.0771
443	1.007	0.0646	0.7641	0.0218	0.3561	0.0802
443	1.007	0.0646	0.7641	0.0218	0.3561	0.0802
520	0.703	0.0208	0.2535	0.0098	0.0816	0.0293
464	0.739	0.0555	0.5183	0.0185	0.2468	0.0734
550	0.864	0.0120	0.2018	0.0063	0.0577	0.0132
421	1.076	0.0620	0.5780	0.0241	0.3708	0.0755
490	0.481	0.0420	0.3861	0.0131	0.1353	0.0572
468	0.669	0.0550	0.5065	0.0173	0.2281	0.0725
555	0.856	0.0105	0.1831	0.0057	0.0548	0.0112
475	0.541	0.0525	0.4628	0.0154	0.1888	0.0701
565	0.791	0.0084	0.1768	0.0046	0.0530	0.0085

The comparison between the empirical results and the modelled reflectance ratios is reasonably good, especially in the concentration range from about 0.03–6 mg Chl-$a\,m^{-3}$. Within this range, the match between the empirical and analytical models is best for the SeaWiFS wavelengths (maximum differences less than 25%), worst for the OCTS wavelengths (maximum differences around 120% at high pigment concentrations) and intermediate for the CZCS wavelengths (maximum errors of about 50% at high pigment concentrations). In the case of the OCTS, the maximum differences are reduced to about 50% if the relative differences are calculated using the empirical algorithm as the reference rather than the model results.

For both the CZCS and the SeaWiFS algorithms, at pigment concentrations less than about 0.02 mg Chl-$a\,m^{-3}$, the empirical algorithms predict higher reflectance ratios than the theory. It is difficult to find a source for these very high reflectance ratios. In the model, as the chlorophyll concentration decreases, the water becomes clearer, and molecular and Raman scatterings by water, with their strong wavelength dependence, become responsible for the dominant blue signal. Addition of any particles with a wavelength dependence for scattering that is less pronounced than that of water would only serve to make the water appear less 'blue'. Therefore, the match between empirical and analytic models at very low pigment concentrations can be improved only if the absorption by phytoplankton pigments or dissolved organic matter, or scattering by particulate matter, are decreased. The deviation between theory and observation at high pigment concentrations is perhaps less surprising, since we had very few measurements of absorption at concentrations greater than 10 mg Chl-$a\,m^{-3}$, and it may be that our parameterization of phytoplankton absorption at high concentrations still requires some refinement.

It is understood that changes in the taxonomic structure of phytoplankton assemblages may modify the relationship between phytoplankton absorption (or attenuation) and concentration of chlorophyll-*a* (Bricaud and Stramski 1990,

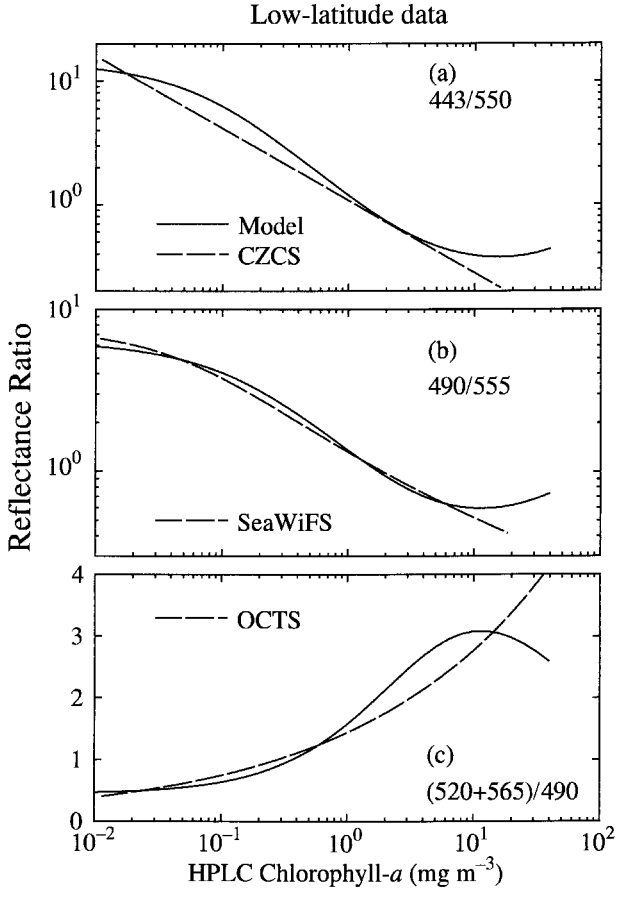

Figure 3. Reflectance ratios computed using the model, plotted as a function of chlorophyll-*a* concentration (continuous line). Wavelength combinations that are used in processing (*a*) CZCS, (*b*) SeaWiFS and (*c*) OCTS data are shown. Also shown in each panel (long dashed line) are the corresponding empirical relationships used for standard processing of data from these satellite sensors.

Hoepffner and Sathyendranath 1992, Mitchell 1992, Fenton *et al.* 1994, Stuart *et al.* 1998). Taxon-dependent variability in the optical properties of phytoplankton absorption may also be responsible for some of the differences between empirical and theoretical algorithms shown in figure 3. This particular aspect of the chlorophyll retrieval problem is examined in some detail in §4, which deals with data from the Labrador Sea.

4. Comparison of model results with data from the Labrador Sea

As mentioned previously, the model of ocean colour presented here was developed using data on phytoplankton absorption collected in low and mid latitudes, because of earlier reports on significant differences in the performance of ocean colour algorithms in polar regions (Mitchell and Holm-Hansen 1991, Mitchell 1992, Sullivan *et al.* 1993, Fenton *et al.* 1994, Dierssen and Smith 2000). In §3, we saw that there was good agreement between the model as implemented and some empirical

algorithms in routine use. Here, we examine the performance of the model in the high-latitude environment of the Labrador Sea.

4.1. *Sampling and data analysis*

The *in situ* radiance and pigment data discussed in this section were collected during two cruises to the Labrador Sea of *CCGS Hudson*: one in October–November 1996 and the other in May–June 1997. Optical observations were made with a Satlantic SeaWiFS Profiling Multichannel Radiometer (SPMR) and SeaWiFS Multichannel Surface Reference (SMSR). Downwelling irradiance $E_d(0, \lambda)$ and upwelling radiance $L_u(0, \lambda)$ were measured just below the sea surface in 13 wavebands: 405, 412, 443, 490, 510, 520, 532, 555, 565, 620, 665, 683 and 700 nm with the SMSR sensors mounted on a floating tethered buoy with an umbilical cable for power and data transmission. The SPMR also has the same 13 channels for vertical profiles of downwelling irradiance $E_d(z, \lambda)$ and upwelling radiance $L_u(z, \lambda)$, and its performance surpasses SeaWiFS sea-truth requirements (McClain *et al.* 1992, Mueller and Austin 1992). It was deployed in a free-fall mode with a Kevlar cable for power and data transmission. Triplicate casts of SPMR were made at each station. The SPMR includes sensors for tilt and pitch, and for pressure. The SMSR and SPMR measurements were always made concurrently and the sensors were deployed 20–100 m from the vessel to avoid ship-shadow effects (Waters *et al.* 1990).

Data collection, corrections and processing for optical observations conformed to SeaWiFS guidelines (Mueller and Austin 1992, 1995). To minimize variability due to clouds and ship-shadow, optical profiles were normally made on overcast or clear days within 2–3 h of solar noon with the sensors on the sunlit side of the vessel. Bio-optical profiles were considered to be reliable if they had no ship-shadow effects, uniform physical and biological properties within well-mixed layers, relatively constant solar irradiance at the surface, and sufficient illumination for irradiance and radiance measurements within the surface mixed layer. Calibrations were performed by the manufacturer at least twice a year. Data processing was accomplished with the manufacturer's Prosoft software which is documented on the Dalhousie University FTP-site address (raptor.ocean.dal.ca). Basic processing included editing the profiles to remove portions with tilts $> 5°$, dark corrections, and binning the data over 1 m intervals. The sampling rate ($6\ s^{-1}$) and profiling speed ($0.8–1.0\ m\ s^{-1}$) resulted in a nominal sampling density of 6–8 measurements of each quantity per metre in the vertical. Only data from the mixed layer of Case 1 stations are used here.

The spectral, diffuse attenuation coefficients for upwelling irradiance, $K_u(\lambda)$, were determined as the slopes of the natural-log transformed profiles of spectral upwelling irradiance. To avoid wave-focusing effects, we typically used 16 1 m bins for each estimate of $K_u(\lambda)$. Upwelling spectral radiance profiles were extrapolated using the $K_u(\lambda)$ values to obtain $L_u(0, \lambda)$, the upwelling radiance just below the sea surface. Sea–air transmittance effects were computed assuming a Fresnel reflectance of 0.021 and a refractive index of 1.345, to obtain the water-leaving radiance. This quantity was then scaled to the ratio of the mean extraterrestrial solar irradiance (Neckel and Labs 1984) at that wavelength to the irradiance at the same wavelength incident at the sea surface, to obtain the normalized water-leaving radiance, $L_{wN}(\lambda)$. These procedures are in accordance with the recommended protocols for SeaWiFS validation (Mueller and Austin 1995).

A CTD/pump cast preceded or followed the optical casts. The CTD/pump system

determined hydrographic and biological structure with conductivity–temperature–pressure (SeaBird), fluorescence (Chelsea Aquatracka) and beam attenuation (SeaTech) sensors. Discrete water samples were collected every 10 m of depth, with a surface sample from 1–5 m depending on sea state. In some cases additional samples were collected from depths corresponding to features of particular interest such as maxima in fluorescence, beam attenuation or density. Triplicate samples from each depth were used to determine chlorophyll-*a* concentration using a Turner fluorometer. In addition, HPLC pigment analyses were also carried out on samples collected at two depths: one in the mixed layer and one below the mixed layer. Sea and sky conditions were documented by photography at all optical stations. The data from the CTD/pump system were used to determine the depth of the mixed layer. In the dataset presented here, the mixed layers were typically greater than 30 m, such that structure in the water column is not likely to influence the water-leaving radiances in any significant manner. Therefore, chlorophyll data obtained from only the top 5 m of the water column are used here. During the 1996 (October–November) cruise to the Labrador Sea, 29 optical stations were occupied, whereas 33 optical stations were occupied in 1997 (May–June). Some five profiles had to be eliminated from each cruise after quality control, and were not used in the analysis presented here.

4.2. *Comparison with model*

Radiance ratios (for the same wavelength groups discussed previously) were computed for the data collected in the Labrador Sea, and are plotted against the measured chlorophyll-*a* concentrations (determined by Turner fluorometry) in figure 4. The reflectance ratios modelled using low and mid latitude data are also plotted on the same figure. The figure shows that there are some systematic differences between the Labrador Sea data and the modelled reflectance ratios, even though the model is in good agreement with the empirical algorithms in common use. This lends further support to earlier reports (Mitchell and Holm-Hansen 1991, Mitchell 1992) that conventional algorithms do not perform satisfactorily in high latitudes, and to the suggestions that there is a need for regional algorithms for interpretation of ocean colour data (Fenton *et al.* 1994).

A possible explanation for this discrepancy lies in the variations in the absorption characteristics of phytoplankton that accompany changes in the phytoplankton community structure. For example, Stuart *et al.* (2000) have reported that diatom blooms and prymnesiophyte blooms were encountered in different parts of the Labrador Sea during a cruise of *CCGS Hudson* in May 1996. They found that there were significant differences between these blooms both in the shapes of the phytoplankton absorption spectra and in the parameters of the function relating absorption coefficient to pigment concentration (phytoplankton samples were separated into two broad groups comprising mostly diatoms or mostly prymnesiophytes, based on the ratios of chlorophyll-c_3 and fucoxanthin to chlorophyll-*a*). We used the same data as Stuart *et al.* (2000) to establish the absorption parameters for diatoms and prymnesiophytes at all the wavelengths of interest in this study (see table 2). Then, we re-ran the reflectance model with these absorption parameters for prymnesiophytes and for diatoms, and the results are also plotted in figure 4. It is seen that the three curves (modelled low-latitude conditions, and modelled prymnesiophyte and diatom blooms) envelope practically all the data points, lending credence to the hypothesis that the variability in the performance of the algorithms may indeed be linked to changes in the phytoplankton community structure.

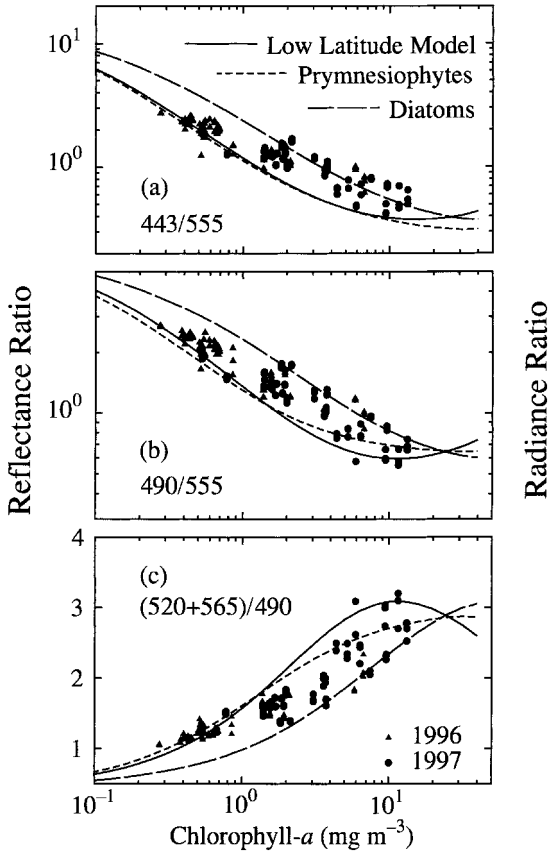

Figure 4. Reflectance ratios plotted as a function of chlorophyll-a concentration, for wavelength combinations used for processing (*a*) CZCS, (*b*) SeaWiFS and (*c*) OCTS data. Continuous line: analytical model developed for low and mid latitudes, as in figure 3. Short dashed lines: variant of the model implemented using absorption characteristics of prymnesiophytes. Long dashed lines: variant of the model implemented using absorption coefficients for diatoms. The absorption properties of both prymnesiophytes and diatoms were measured in blooms encountered in the Labrador Sea (Stuart *et al.* 2000). Triangles: *in situ* data on radiance ratios at the sea surface measured during a cruise to the Labrador Sea in October 1996. Filled circles: *in situ* data on radiance ratios measured during a cruise to the Labrador Sea in May 1997. Note that the axes are the same for reflectance ratios and radiance ratios. Note also that 555 nm was used instead of 550 nm for computing the CZCS-type ratios from the *in situ* observations, since the instrumentation did not have a 550 nm channel.

The absorption parameters for diatoms and prymnesiophytes used in the model were derived from data collected in May 1996, whereas the *in situ* optical data presented here were collected during October–November 1996 and May–June 1997. During the latter two cruises, no distinct blooms were encountered as in May 1996: the HPLC data suggested that the populations were mostly mixed, with some evidence of the presence of diatoms and prymnesiophytes in the populations. We used the HPLC data to identify stations where diatoms dominated the assemblage. If the HPLC sample for a station was characterized by relatively low concentrations of chlorophyll-c_3 (chl-c_3:chl-*a* ratio < 0.02) and relatively high concentrations of

fucoxanthin (fuco:chl-*a* ratio > 0.4), then those stations were identified as diatom-dominated stations. Only these stations are plotted on figure 5. It is very encouraging to note that all these diatom-dominated stations lie on, or close to, the curve for the diatom variant of the model.

It is interesting to note that the prymnesiophyte model behaves very much like the low-latitude model. This implies that, in such blooms, we need not anticipate that the standard algorithms may be in error, even in the high-latitude environment of the Labrador Sea. Thus, it would perhaps be more correct to say that the performance of the standard algorithms may be questionable in the presence of some diatom blooms, whether they be in high latitudes or not. On the other hand, the fact that the type of discrepancy discussed here has been noted so often in high latitudes perhaps indicates that such blooms are likely to occur more often in high latitudes than elsewhere.

5. Sensitivity analyses

5.1. *Yellow substances*

In the previous section we identified species changes as a possible cause of variation in the relationship between ocean colour signals and pigment concentration.

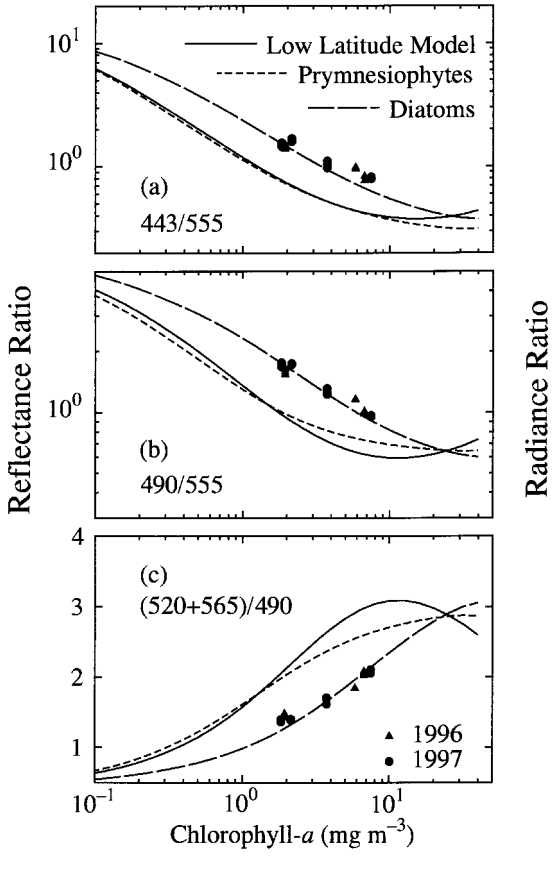

Figure 5. The same as figure 4, except that only data from October 1996 and May 1997 stations identified as being *diatom-dominated* (based on HPLC data) are plotted.

Another potential candidate for this variability is change in the absorption by yellow substances relative to that by phytoplankton pigments. Figure 6 shows the relationship between reflectance ratios and chlorophyll-*a* concentration, for absorption by yellow substances relative to phytoplankton absorption at 440 nm ranging from 0 to 200%. Note that increasing the absorption by yellow substances renders the water darker in the blue and green parts of the spectrum, with a consequent decrease in the blue–green ratios used in CZCS and SeaWiFS algorithms, and an increase in the OCTS ratio. This is in the opposite direction to the change noted for diatom blooms: the large diatom cells tend to absorb less per unit pigment concentration than smaller phytoplankton cells, such that waters with diatom cells are brighter and bluer than waters with a population of smaller cells having the same pigment concentration. The standard runs of the model were made assuming that absorption

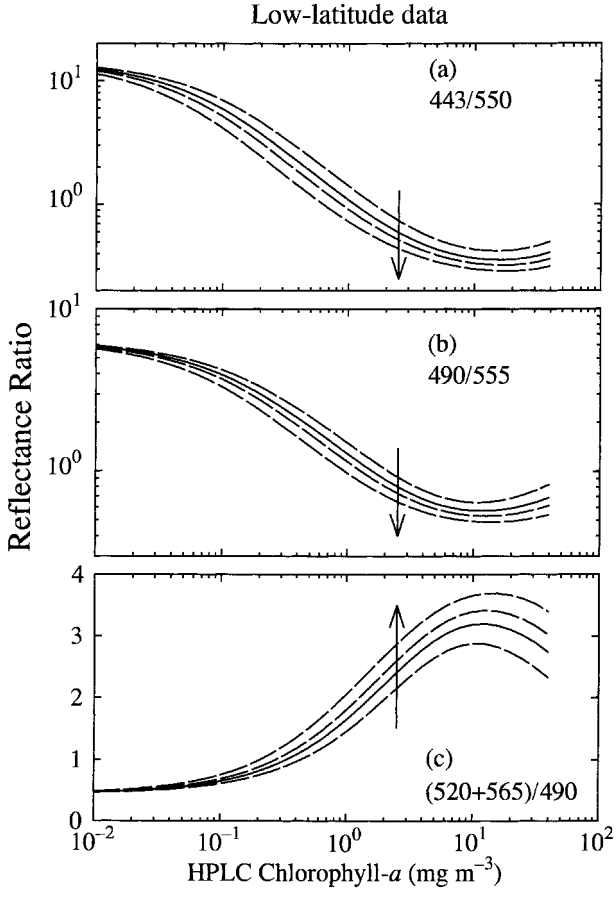

Figure 6. Reflectance ratios computed using the model, plotted as a function of chlorophyll-*a* concentration. Wavelength combinations that are used in processing (*a*) CZCS, (*b*) SeaWiFS and (*c*) OCTS data are shown. Continuous line: results from the standard run of the model, as implemented for low and mid latitudes (this curve is the same as the continuous line in figure 3). Dashed lines: results of model runs when the proportion of absorption by yellow substances at 440 nm was set to 0, 100, and 200% of absorption by phytoplankton at the same wavelength. The arrows indicate the direction which the computed values move, with increasing absorption by yellow substances.

by yellow substances amounted to 30% of absorption by phytoplankton cells at 440 nm. Decreasing this proportion changes the signals in the right direction for explaining the observations in the Labrador Sea, but it is not sufficient, even if the proportion of yellow substance is reduced to zero (figure 6).

5.2. *Raman scattering*

We have incorporated Raman scattering into the model and it is interesting to examine the effect this has on the algorithms. Figure 7 shows that running the model with or without Raman scattering had little effect on the algorithms discussed here. This is surprising since it has been noted in a number of recent papers that Raman scattering has a significant effect on reflectance values in waters with low pigment concentration (see, for example, works by Stavn and Weidemann (1988), Marshall and Smith (1990) and Haltrin *et al.* (1997)). The explanation lies in the fact that the relative increase in the ocean colour signal due to Raman scattering as modelled here remains fairly constant at the wavelengths used in these algorithms (figure 8), such that the net effect becomes negligible when ratios of the signal at these wavelengths are calculated.

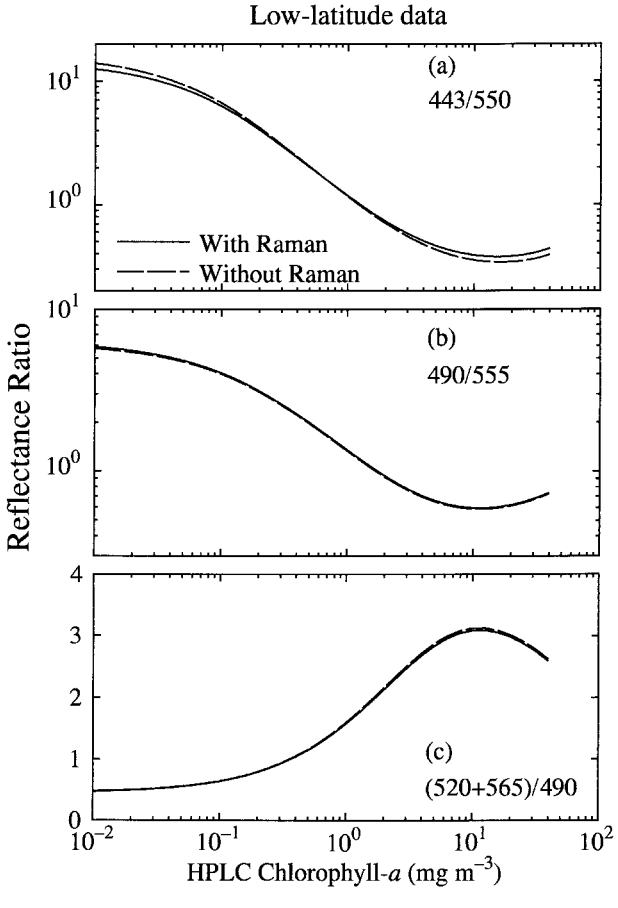

Figure 7. As figure 6, but dashed lines represent results of model runs when Raman scattering is switched off.

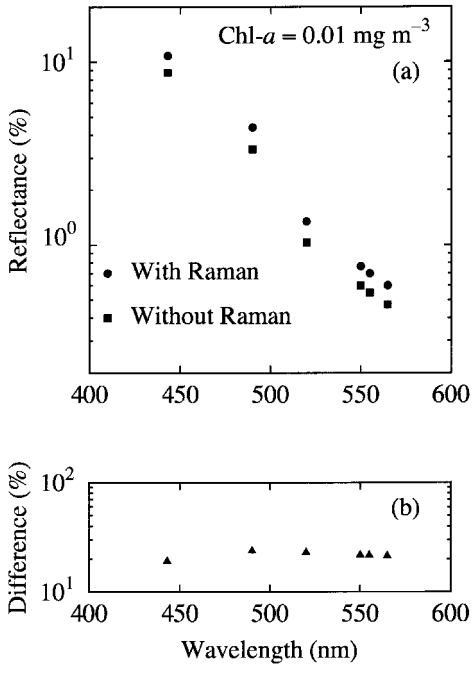

Figure 8. (*a*) Reflectance values computed for a chlorophyll-*a* concentration of 0.01 mg Chl-*a* m^{-3}, plotted as a function of wavelength. Circles: computations that include Raman scattering. Squares: computations that ignore Raman scattering. (*b*) Difference in the two computed reflectances shown in (*a*), plotted as a function of wavelength.

5.3. *Particle scattering*

Because the model of Sathyendranath *et al.* (1989) was intended for application in coastal waters, they separated particle scattering into two components: a part that was associated with chlorophyll-*a* and another component that varied independently of it. In the model presented here, which is designed for Case 1 waters, we have only one component for particle scattering: all the characteristics of particle scattering (magnitude, total scattering to backscattering ratio and wavelength dependence) are tied to chlorophyll-*a* concentration. The wavelength dependence for particle scattering used here (equations (8) and (9)) varies from λ^{-2} for a chlorophyll-*a* concentration of 0.01 mg chl-*a* m^{-3} to λ^{2} for a chlorophyll-*a* concentration of 100 mg chl-*a* m^{-3}.

To examine the sensitivity of the model to these assumptions, we also ran the model assuming no wavelength dependence for b_p (power of λ dependence = 0). Comparison of the results shows (figure 9) that the assumptions regarding the wavelength dependence of b_p affect the results only at pigment concentrations greater than 1 mg chl-*a* m^{-3}. The results of model runs with the variable power dependence are more in accordance with the empirical results. Hence, it appears desirable to retain this in the model, even though the range in the power is greater than what one would expect based on arguments regarding the Junge-type particle size distribution in oceanic waters.

We also examined the influence of particle scattering on the reflectance ratios by computing the extreme case of no particle backscattering whatsoever. The results are plotted in figure 9. Decreasing particle scattering clearly has a significant effect, and this effect is in the right sense to explain the discrepancies observed in high

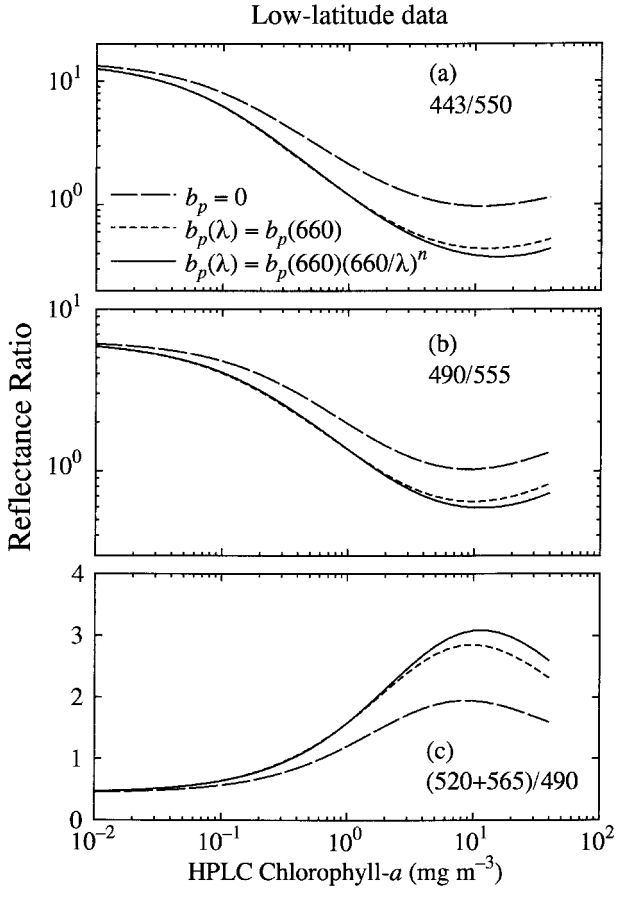

Figure 9. Reflectance ratios computed using the model, plotted as a function of chlorophyll-*a* concentration. Wavelength combinations that are used in processing (*a*) CZCS, (*b*) SeaWiFS and (*c*) OCTS data are shown. Continuous line: results from the standard run of the model, as implemented for low and mid latitudes (this curve is the same as the continuous line in figure 3). Short dashed line: same as the continuous line, with the exception that the wavelength dependence of particle scattering (b_p) is assumed to be neutral. Long dashed line: same as the continuous line, with the exception that particle scattering is set to zero.

latitudes. Note that, in the model used here, particle scattering per unit pigment concentration (b_p/C) and particle backscattering efficiency ($\tilde{b}_{bp}$) decrease with increasing pigment concentration. Therefore, in this sensitivity analysis, we are looking at the effect of a further decrease in particle backscattering, over and above what is treated here as being the common trend. We have no observations to support this hypothesis for the Labrador Sea, but if the diatom blooms backscattered markedly less than other phytoplankton populations of similar concentrations (see Dierssen and Smith 2000), then one might anticipate that the species-dependent changes in ocean colour would be enhanced.

5.4. *Parameterization of phytoplankton absorption*

We have used a purely empirical relationship to describe the dependence of phytoplankton absorption on concentration of chlorophyll-*a*. It is not an ideal

function to fit to absorption data (Lutz *et al.* 1996) since the slope of the curve approaches zero asymptotically at high pigment concentrations. We recognize that the mismatch between empirical relationships and the model at high pigment concentrations may be attributed at least partially to the inadequacy of the fitted relationship between absorption and pigment data. The problem is perhaps exacerbated by the fact that we have very few measurements at high concentrations (see figure 2), such that the fitting programme is constrained less in this range.

To examine whether the function selected to describe this relationship has an important impact on the results, we fitted another, commonly used power equation of the type $a_c(\lambda) = pC^q$ to our low and mid latitude data, and then re-ran the model with this parameterization of phytoplankton absorption (results not shown). The power function brought the slope of the results more in line with the slope of the empirical results for high chlorophyll concentrations. On the other hand, at the low-concentration end, this equation increased differences between model and empirical relationships, in the case of CZCS and SeaWiFS algorithms. Lutz *et al.* (1996) have also pointed out that the power function is not a perfect choice for describing absorption data at low pigment concentration.

We therefore tried yet another function to describe phytoplankton absorption as a function of chlorophyll-*a* concentration. The function was developed by starting with some reasonable yet simple assumptions about phytoplankton populations. We first assumed that the total chlorophyll-*a* was made up of chlorophyll-*a* in two distinct populations of phytoplankton: one with a high specific absorption coefficient, which was incapable of growing beyond a certain concentration, and another with a lower specific absorption coefficient which was capable of growth to high concentrations. We parameterized the concentration C_1 of the first population as a function of total concentration C, by setting: $C_1 = C_1^{max}[1 - \exp(-SC)]$, where C_1^{max} and S are unknown parameters. It automatically follows that the concentration of the second population is $C_2 = C - C_1$. If we now admit that the two populations have specific absorption coefficients, a_1^* and a_2^* respectively, then we have $a_p(\lambda) = a_1^*(\lambda)C_1 + a_2^*(\lambda)C_2$. Substituting for C_1 and C_2 and simplifying yields:

$$a_p(\lambda) = C_1^{max}[a_1^*(\lambda) - a_2^*(\lambda)][1 - \exp(-SC)] + Ca_2^*(\lambda) \qquad (13)$$

This equation has three free parameters at each wavelength: S, a_2^* and $C_1^{max}[a_1^*(\lambda) - a_2^*(\lambda)]$, which we can set equal to a composite parameter, say U.

We fitted equation (13) to our low and mid latitude data. The fitted parameters are listed in table 3. When the reflectance model was run with this model for phytoplankton absorption (figure 10), the relationships between reflectance ratios and pigment concentration became monotonic for the entire range of pigment concentrations considered here, unlike the results for the Michaelis–Menten type of model for phytoplankton absorption (equation (12)). This brought the model results for high pigment concentrations closer to the empirical results in the case of CZCS and SeaWiFS algorithms, but it pulled the model further away from the empirical results in the case of the OCTS algorithm.

We also fitted equation (13) to our data on blooms of diatoms and prymnesiophytes. Since the bloom data did not have many observations at low concentrations, we had to apply some constraints to avoid fitting physically untenable parameters. We obtained fairly reasonable results (see table 4) when we fixed an upper limit for S of 2 (in which we were guided by the fact that the low latitude data did not yield any values of S greater than 1.5, and also by the quality of the fits at low

Table 3. The parameters U (m^{-1}), a_2^* (m^2 mg(Chl-a)$^{-1}$) and S (m^3 (mg Chl-a)$^{-1}$) of equation (13) for low and mid latitude datasets, as a function of wavelength. Parameter values are given for each of the wavelengths used in the algorithms presented here (lower member of each pair), and for their corresponding Raman wavelengths (upper member).

λ (nm)	U	a_2^*	S
386	0.07551	0.02417	0.5777
443	0.07318	0.02626	0.9951
443	0.07318	0.02626	0.9951
520	0.02051	0.01194	0.8779
464	0.06182	0.02091	1.0648
550	0.00708	0.00887	1.1296
421	0.08412	0.02544	0.7035
490	0.04806	0.01449	1.0319
468	0.06077	0.01980	1.0933
555	0.00569	0.00805	1.1615
475	0.05773	0.01731	1.1142
565	0.00400	0.00665	1.0706

concentrations). However, for some wavelengths in the case of the prymnesiophytes, the parameter a_2^* became zero, such that the fitted curves for those wavelengths had the same saturating form that was seen to be a drawback of the Michaelis–Menten equation. When the reflectance models are run with these new parameterizations of the two blooms, we see (figure 11) that all the model curves are now monotonic, except for two of the prymnesiophyte curves that use the wavelengths for which a_2^* is zero. Since the maximum concentrations observed during the prymnesiophyte bloom were less than 5 mg Chl-a m^{-3}, it is possible that the extrapolations for this population to high concentrations are not realistic.

With the exception of a couple of wavelengths for the prymnesiophyte bloom, the new model for phytoplankton absorption avoids the saturation in absorption at high pigment concentrations that is a feature of the Michaelis–Menten model. This is an advantage, but the new model also has some drawbacks. The retrieved parameter U, which is a composite parameter, is not easily interpreted. According to the assumptions used to develop the model, the parameter S should be wavelength independent; in practice, it does not always emerge as such (see tables 3 and 4).

The main thing we wish to point out here is that there are some uncertainties in the reflectance model which arise from uncertainties in the parameterization of phytoplankton absorption. These problems are most pronounced at high concentrations, where we have the additional problem of not having a great number of observations to constrain models better.

6. Discussion and conclusion

In this paper we have presented a semi-empirical model of ocean colour reflectance, implemented using absorption characteristics of phytoplankton from mid and low latitudes. The results are in good agreement with those of empirical algorithms in use today for processing satellite-derived ocean colour data.

When the model is compared with ocean colour data from the Labrador Sea, an offset in the data emerges. This can be explained if the variability in the absorption

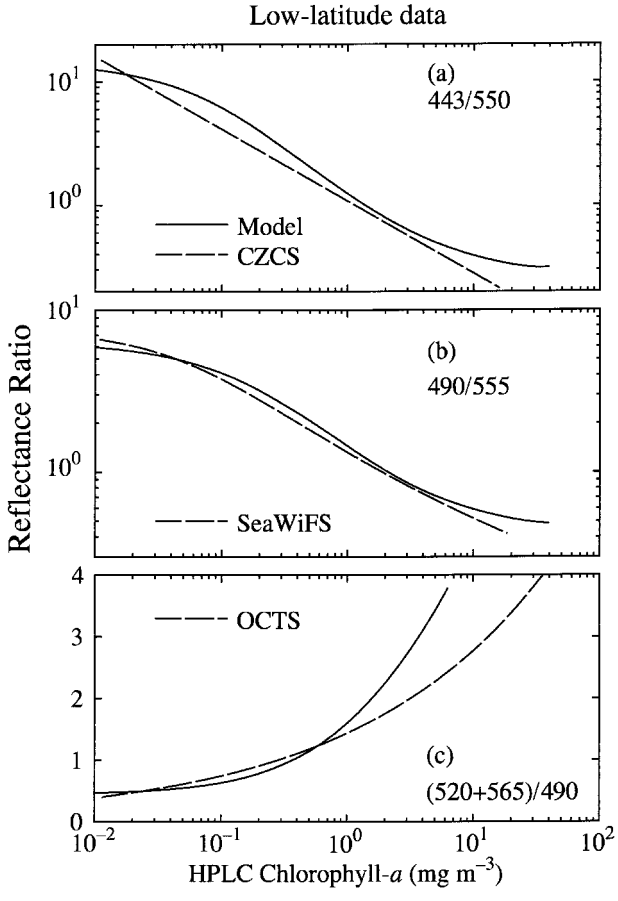

Figure 10. Reflectance ratios computed using the model, plotted as a function of chlorophyll-*a* concentration (continuous line). The model computations in this figure are the same as those used in figure 3, with the only difference that equation (13) was used to parameterize phytoplankton absorption. Wavelength combinations that are used in processing (*a*) CZCS, (*b*) SeaWiFS and (*c*) OCTS data are shown. Also shown in each panel (long dashed line) are the corresponding empirical relationships used for standard processing of data from these satellite sensors.

properties of phytoplankton populations encountered in these waters is accounted for. Such effects of phytoplankton population variability on ocean colour algorithms may be enhanced if populations of phytoplankton with low absorption efficiencies are also associated with lower than usual coefficients for backscattering by particulate matter. The effect of increasing yellow substances is in the opposite sense to the effect of decreasing absorption efficiencies for phytoplankton.

These observations suggest that algorithms tuned to match the optical properties of local phytoplankton have the potential to perform better than a universal algorithm applied indiscriminately to the entire global ocean. Indeed, Carder *et al.* (1999) noted a significant reduction in algorithm errors when MODIS algorithms were parameterized for three different bio-optical domains, in an effort to account for variations in pigment-to-chlorophyll ratio and pigment packaging. Ideally, it would be possible to use satellite data to distinguish between major phytoplankton groups

Table 4. The parameters U (m^{-1}), a_2^* (m^2 mg(Chl-a)$^{-1}$) and S (m^3 (mg Chl-a)$^{-1}$) of equation (13) for two datasets, as a function of wavelength. Parameter values are given for each of the wavelengths used in the algorithms presented here (lower member of each pair), and for their corresponding Raman wavelengths (upper member). Note that 2.0 was the upper limit set for S in the fitting routine, and that 0.0 was the lower limit set for a_2^*.

	Diatom bloom			Prymnesiophyte bloom		
λ (nm)	U	a_2^*	S	U	a_2^*	S
386	0.02123	0.01498	2.0	0.01602	0.03526	2.0
443	0.01180	0.01565	2.0	0.02775	0.03771	2.0
443	0.01180	0.01565	2.0	0.02775	0.03771	2.0
520	0.00680	0.00626	2.0	0.05447	0.0	0.5075
464	0.01058	0.01237	2.0	0.04037	0.02489	1.4613
550	0.00416	0.00431	2.0	0.00485	0.00605	2.0
421	0.01699	0.01489	2.0	0.02339	0.03882	2.0
490	0.00701	0.00889	2.0	0.09295	0.0	0.5719
468	0.01048	0.01173	2.0	0.04589	0.02166	1.2596
555	0.00374	0.00390	2.0	0.00324	0.00596	2.0
475	0.00715	0.01080	2.0	0.08635	0.00798	0.6944
565	0.00282	0.00332	2.0	0.00238	0.00493	2.0

based on changes in their pigment composition, but the simple ratio algorithms that are discussed in this paper clearly do not have the capability to achieve this refinement. However, this is certainly worth striving for: the new and improved ocean colour data streams that provide information on water-leaving radiances at many more wavelengths than the CZCS certainly improve the chances of attaining this goal.

The results presented here highlight the usefulness of collecting information on the optical characteristics of various, naturally occurring phytoplankton assemblages. It is also important to have this information for the entire range of pigment concentrations that may be encountered. In our own dataset, the parameterization of phytoplankton absorption characteristics at high pigment concentrations is based on a small number of data points. The resultant uncertainties in the fitted parameters are a possible reason for the residual discrepancies between the model and empirical relationships at high concentrations. Another possibility is that there are changes in the backscattering characteristics and in the relative absorption by yellow substances that are not accounted for in the model. These remaining questions can be resolved only when more optical data become available at high pigment concentrations.

Acknowledgments

We thank Carla Caverhill for helpful comments on the manuscript. The work presented in this paper was supported by the Office of Naval Research, and National Aeronautics and Space Administration, USA; the Department of Fisheries and Oceans, Canada; the Natural Sciences and Engineering Research Council, Canada and NASDA (National Space Development Agency of Japan), Japan. This work was carried out as part of the Canadian contribution to the Joint Global Ocean Flux Study.

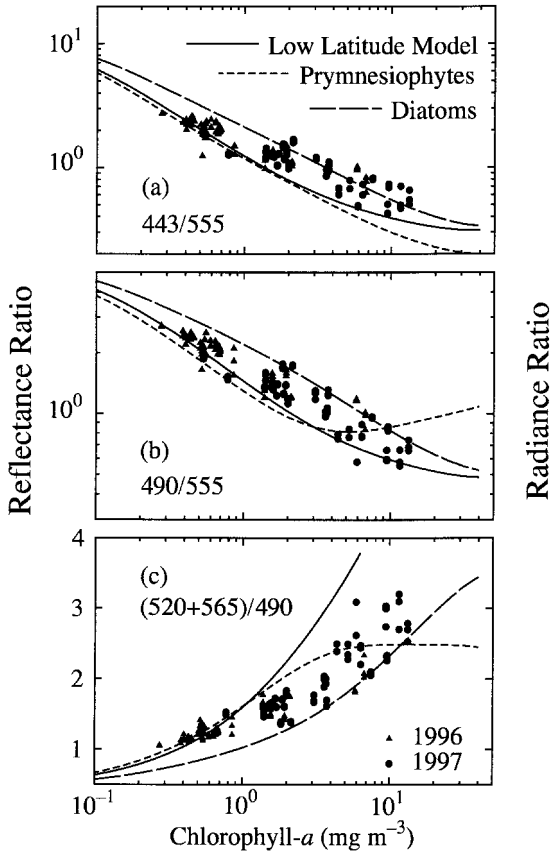

Figure 11. Reflectance ratios plotted as a function of chlorophyll-*a* concentration, for wavelength combinations used for processing (*a*) CZCS, (*b*) SeaWiFS and (*c*) OCTS data. The model computations in this figure are the same as those used in figure 4, with the only difference that equation (13) was used to parameterize phytoplankton absorption. Continuous line: analytical model developed for low and mid latitudes, same as in figure 10. Short dashed lines: variant of the model implemented using absorption characteristics of prymnesiophytes. Long dashed lines: variant of the model implemented using absorption coefficients for diatoms. The absorption properties of both prymnesiophytes and diatoms were measured in blooms encountered in the Labrador Sea (Stuart *et al.* 2000). Triangles: *in situ* data on radiance ratios measured during a cruise to the Labrador Sea in October 1996. Filled circles: *in situ* data on radiance ratios measured during a cruise to the Labrador Sea in May 1997. Note that the axes are the same for reflectance ratios and radiance ratios.

References

Åas, E., 1987, Two-stream irradiance model for deep waters. *Applied Optics*, **26**, 2095–2101.

Bader, H., 1970, The hyperbolic distribution of particle sizes. *Journal of Geophysical Research*, **75**, 2822–2830.

Bartlett, J. S., Voss, K. L., Sathyendranath, S., and Vodacek, A., 1998, Raman scattering by pure water and seawater. *Applied Optics*, **37**, 3324–3332.

Bricaud, A., Morel, A., and Prieur, L., 1981, Absorption by dissolved organic matter of the sea (yellow substance) in the UV and visible domains. *Limnology and Oceanography*, **26**, 43–53.

Bricaud, A., and Stramski, D., 1990, Spectral absorption coefficients of living phytoplankton and nonalgal biogenous matter: a comparison between the Peru upwelling area and the Sargasso Sea. *Limnology and Oceanography*, **35**, 562–582.

Brun-Cottan, J. C., 1971, Etude de la granulomrie des particules marines. Mesures effectuées avec un compteur Coulter. *Cahiers Océanographiques*, **23**, 193–205.

Carder, K. L., Chen, F. R., Lee, Z. P., Hawes, S. K., and Kamykowski, D., 1999, Semianalytic Moderate-Resolution Imaging Spectrometer algorithms for chlorophyll *a* and absorption with bio-optical domains based on nitrate-depletion temperatures. *Journal of Geophysical Research*, **104**, 5403–5421.

Ciotti, A. M., Cullen, J. J., and Lewis, M. R., 1999, Asemi-analytical model of the influence of phytoplankton community structure on the relationship between light attenuation and ocean color. *Journal of Geophysical Research*, **104**, 1559–1578.

Dierssen, H. M., and Smith, R. C., 2000, Bio-optical properties and remote sensing ocean color algorithms for Antarctic coastal waters. *Journal of Geophysical Research*, in press.

Fenton, N., Priddle, J., and Tett, P., 1994, Regional variations in bio-optical properties of the surface waters in the Southern Ocean. *Antarctic Science*, **6**, 443–448.

Gordon, H. R., 1989, Dependence of the diffuse reflectance of natural waters on the sun angle. *Limnology and Oceanography*, **34**, 1484–1489.

Gordon, H. R., Brown, O. B., and Jacobs, M. M., 1975, Computed relationships between the inherent and apparent optical properties of a flat, homogeneous ocean. *Applied Optics*, **14**, 417–427.

Gordon, H. R., Clark, D. K., Brown, J. W., Brown, O. B., Evans, R. H., and Broenkow, W. W., 1983, Phytoplankton pigment concentrations in the Middle Atlantic Bight: comparison of ship determinations and CZCS estimates. *Applied Optics*, **22**, 20–36.

Gordon, H. R., and Morel, A., 1983, *Remote Assessment of Ocean Color for Interpretation of Satellite Visible Imagery. A Review* (New York: Springer-Verlag).

Haltrin, V. I., Kattawar, G. W., and Weideman, A. D., 1997, Modeling of elastic and inelastic scattering effects in oceanic optics. In *Ocean Optics* XIII, edited by S. G. Ackleson and R. Frouin, *Proceedings of SPIE*, **2963**.

Head, E. J. H., and Horne, E. P. W., 1993, Pigment transformation and vertical flux in an area of convergence in the North Atlantic. *Deep-Sea Research II*, **40**, 329–346.

Hoepffner, N., and Sathyendranath, S., 1992, Bio-optical characteristics of coastal waters: absorption spectra of phytoplankton and pigment distribution in the western North Atlantic. *Limnology and Oceanography*, **37**, 1660–1679.

Jonasz, M., 1983, Particle-size distributions in the Baltic. *Tellus B*, **35**, 346–358.

Kirk, J. T. O., 1984, Dependence of relationship between inherent and apparent optical properties of water on solar altitude. *Limnology and Oceanography*, **29**, 350–356.

Kirk, J. T. O., 1989, The upwelling light stream in natural waters. *Limnology and Oceanography*, **34**, 1410–1425.

Kishino, M., Ishimaru, T., Furuya, K., Oishi, T., and Kawasaki, K., 1995, *Development of Under Water Algorithm* (Saitama, Japan: The Institute of Physical and Chemical Research), in Japanese.

Loisel, H., and Morel, A., 1998, Light scattering and chlorophyll concentration in case 1 waters: a reexamination. *Limnology and Oceanography*, **43**, 847–858.

Lutz, V. A., Sathyendranath, S., and Head, E. J. H., 1996, Absorption coefficient of phytoplankton: regional variations in the North Atlantic. *Marine Ecology Progress Series*, **135**, 197–213.

Marshall, B. R., and Smith, R. C., 1990, Raman scattering and in-water ocean optical properties. *Applied Optics*, **29**, 71–84.

McClain, C. R., Esaias, W. E., Barnes, W., Guenther, B., Endres, D., Hooker, S., Mitchell, G., and Barnes, R., 1992, *SeaWiFS Calibration and Validation Plan* (Greenbelt, Maryland: NASA Technical Memorandum No. 104566, vol. 3).

Mitchell, B. G., 1992, Predictive bio-optical relationships for polar oceans and marginal ice zones. *Journal of Marine Systems*, **3**, 91–105.

Mitchell, B. G., and Holm-Hansen, O., 1991, Bio-optical properties of Antarctic Peninsula waters: differentiation from temperate ocean models. *Deep-Sea Research*, **38**, 1009–1028.

Morel, A., 1973, Diffusion de la lumière par les eaux de mer. Résultats expérimentaux et approche théorique. In *AGARD Lecture Series No. 61, Optics of the Sea (Interface and In-water Transmission and Imaging)* (London: North Atlantic Treaty Organisation).

Morel, A., 1974, Optical properties of pure seawater. In *Optical Aspects of Oceanography*, edited by N. G. Jerlov and E. Steemann Nielsen (New York: Academic), pp. 1–24.

Morel, A., 1980, In-water and remote measurement of ocean color. *Boundary-Layer Meteorology*, **18**, 177–201.

Morel, A., and Gentili, B., 1991, Diffuse reflectance of oceanic waters: its dependence on sun angle as influenced by the molecular scattering contribution. *Applied Optics*, **30**, 4427–4438.

Morel, A., and Gentili, B., 1993, Diffuse reflectance of oceanic waters. II Bidirectional aspects. *Applied Optics*, **32**, 6864–6879.

Morel, A., and Prieur, L., 1977, Analysis of variations in ocean color. *Limnology and Oceanography*, **22**, 709–722.

Mueller, J. L., and Austin, R. W., 1992, *Ocean Optics Protocols for SeaWiFS Validation* (Greenbelt, Maryland: NASA Technical Memorandum, No. 104566, vol. 5).

Mueller, J. L., and Austin, R. W., 1995, *Ocean Optics Protocols for SeaWiFS Validation, Revision 1* (Greenbelt, Maryland: NASA Technical Memorandum 104566, vol. 25).

NASDA, 1997, *Advanced Earth Observing Satellite (ADEOS), OCTS Data Processing Algorithm Description, Version 2.0.1* (Tokyo: NASDA Earth Observation Center).

Neckel, H., and Labs, D., 1984, The solar radiation between 3300 and 12 500 Å. *Solar Physics*, **90**, 205–258.

O'Reilly, J. E., Maritorena, S., Mitchell, B. G., Siegel, D. A., Carder, K. L., Garver, S. A., Kahru, M., and McClain, C., 1998, Ocean color chlorophyll algorithms for SeaWiFS. *Journal of Geophysical Research*, **103**, 24 937–24 953.

Platt, T., Lewis, M., and Geider, R., 1984, Thermodynamics of the pelagic ecosystem: elementary closure conditions for biological production in the open ocean. In *Flows of Energy and Materials in Marine Ecosystems*, edited by M. J. R. Fasham (New York: Plenum).

Pope, R. M., and Fry, E. S., 1997, Absorption spectrum (380–700 nm) of pure water: II. Integrating cavity measurements. *Applied Optics*, **36**, 8710–8723.

Prieur, L., and Sathyendranath, S., 1981, An optical classification of coastal and oceanic waters based on the specific spectral absorption curves of phytoplankton pigments, dissolved organic matter, and other particulate materials. *Limnology and Oceanography*, **26**, 671–689.

Sathyendranath, S., and Morel, A., 1983, Light emerging from the sea—interpretation and uses in remote sensing. In *Remote Sensing Applications in Marine Science and Technology*, edited by A. P. Cracknell (Dordrecht: Reidel).

Sathyendranath, S., and Platt, T., 1989, Remote sensing of ocean chlorophyll: consequence of non-uniform pigment profile. *Applied Optics*, **28**, 490–495.

Sathyendranath, S., and Platt, T., 1997, Analytic model of ocean color. *Applied Optics*, **36**, 2620–2629.

Sathyendranath, S., and Platt, T., 1998, Ocean-colour model incorporating transspectral processes. *Applied Optics*, **37**, 2216–2227.

Sathyendranath, S., Prieur, L., and Morel, A., 1989, A three-component model of ocean colour and its application to remote sensing of phytoplankton pigments in coastal waters. *International Journal of Remote Sensing*, **10**, 1373–1394.

Sathyendranath, S., Stuart, V., Irwin, B. D., Maass, H., Savidge, G., Gilpin, L., and Platt, T., 1999, Seasonal variations in bio-optical properties of phytoplankton in the Arabian Sea. *Deep-Sea Research*, **46**, 633–654.

Sheldon, R. W., Prakash, A., and Sutcliffe, W. H., 1972, The size distribution of particles in the ocean. *Limnology and Oceanography*, **17**, 327–340.

Stavn, R. H., and Weidemann, A. D., 1988, Raman scattering effects in ocean optics. *Proceedings of SPIE, Ocean Optics IX*, **925**, 131–139.

Stuart, V., Sathyendranath, S., Head, E. J. H., Platt, T., Irwin, B., and Maass, H., 2000, Bio-optical characteristics of diatom and prymnesiophyte populations in the Labrador Sea. *Marine Ecology Progress Series*, in press.

STUART, V., SATHYENDRANATH, S., PLATT, T., MAASS, H., and IRWIN, B. D., 1998, Pigments and species composition of natural phytoplankton populations: effect on the absorption spectra. *Journal of Plankton Research*, **20**, 187–217.

SULLIVAN, C. W., ARRIGO, K. R., MCCLAIN, C. R., COMISO, J. C., and FIRESTONE, J., 1993, Distributions of phytoplankton blooms in the Southern Ocean. *Science*, **262**, 1832–1837.

ULLOA, O., SATHYENDRANATH, S., and PLATT, T., 1994, Effect of the particle–size distribution on the backscattering ratio in seawater. *Applied Optics*, **33**, 7070–7077.

WATERS, K. J., SMITH, R. C., and LEWIS, M. R., 1990, Avoiding ship-induced light-field perturbation in the determination of oceanic optical properties. *Oceanography*, **3**, 18–21.